Article citation info:
MITURA A, GAWRYLUK J, TETER A. Numerical and experimental studies on the rotating rotor with three active composite blades. Eksploatacja i Niezawodnosc – Maintenance and Reliability 2017; 19 (4): 571–579, http://dx.doi.org/10.17531/ein.2017.4.11.

Andrzej MITURA
Jarosław GAWRYLUK
Andrzej TETER

NUMERICAL AND EXPERIMENTAL STUDIES ON THE ROTATING ROTOR WITH THREE ACTIVE COMPOSITE BLADES

BADANIA NUMERYCZNE I EKSPERYMENTALNE WIRUJĄCEGO WIRNIKA Z TRZEMA AKTYWNYMI ŁOPATAMI KOMPOZYTOWYMI

In this paper, the dynamic behaviour of active composite blades were considered. Both numerical and experimental studies were performed. It was assumed that the rotor hub would be rotated at constant velocity. Experimental measurements were made. A special test rig was built which consisted of an active rotor with three composite blades, an electric drive system and a system of Digital Signal Processors. This DSP system was used for the excitation of the blades, control of the hub's rotary velocity and data acquisition. The MFC patch and strain-gauge sensors were used. The influence of the hub's rotary velocity and/or piezoelectric effect on the dynamic behaviour of the blades was determined. The numerical simulations were performed using two commercial simulation programmes: Abaqus and Matlab.

***Keywords**: MFC actuator, laminate, stiffening effect, softening effect, FEM.*

W niniejszej pracy przedstawiono dynamikę aktywnych łopat kompozytowych. Przeprowadzono badania numeryczne i eksperymentalne. Założono, że wirnik obraca się ze stałą prędkością obrotową. Pomiary doświadczalne wykonano na stanowisku badawczym, składającym się z aktywnego wirnika z trzema łopatami, elektrycznego układu napędowego oraz procesora sygnałowego DSP. Układ elektroniczny z procesorem wykorzystano do wzbudzania łopat, kontroli prędkości obrotowej oraz pozyskania danych pomiarowych. W badaniach laboratoryjnych użyto elementy aktywne typu MFC oraz czujniki tensometryczne. W pracy określono wpływ prędkości obrotowej piasty oraz efektu piezoelektrycznego na dynamikę łopat. Symulacje numeryczne przeprowadzono z zastosowaniem programów: Abaqus oraz Matlab.

***Słowa kluczowe**: Aktywator MFC, laminat, efekt usztywniający, efekt zmiękczający, MES.*

1. Introduction

Systems with rotating blades are used in many engineering applications. Composite blades can be used in a drone, a helicopter, a wind turbine and many others. Active rotors are the most interesting because one can change the dynamic behavior of such structures in the real time. In the literature of the subject, one can find many solutions for active rotor design. More details can be found in the monograph by Chopra and Sirohi [6]. The researchers from the Department of Applied Mechanics at the Lublin University of Technology, Poland, built the experimental setup of a rotor with three composite blades. In the paper [16], the experimental modal analysis and the numerical modal analysis of this stand were compared. The experimental study was performed by two independent methods. The first was the non-contact method. To this end, a laser vibrometer system was used. The other was the contact method, where an acceleration sensor and a modal hammer were applied. The experimental results were compared with numerical modal analysis performed by the finite element method using the Abaqus software. In this study, the rotor was fixed. Therefore, the influence of the rotor's rotational velocity on the behaviour of the blades was not examined. The relationship of natural frequency versus rotational velocity of the rotor is discussed in the papers [5,17] for a wind turbine blade and a helicopter blade, respectively. The finite element method was applied. In the literature, authors did not find experimental validation of this type solutions. The main problem lies in the experimental verification of numerical results for rotating structures. The rotating structures create difficulties in the implementation of the measurement system. NASA [4] presents the solution dedicated to rotating blades. In a rotating system the vibration of the blades was detected by strain-gauges and optical motion sensors. Special 100 channels slip ring assembly for strain-gauge leads were mounted at the bottom of the multi-blade rotor. The authors of this paper presented their test stand, where a similar solution with slip rings was applied. It enabled performing tests with non-zero rotational velocity.

Experimental studies of active blades can be conducted using piezoelectric (PZT) elements, the so-called Macro Fiber Composite (MFC) elements [15]. Such elements can be used as actuators or sensors. More information about these elements can be found in the papers [2, 12, 14] or books [3,6]. An interesting problem concerns the impact of the stiffening effect on the natural frequencies of the laminated beam with piezoelectric actuators. Kuo [9] indicated that piezoelectric elements can be used to increase or decrease the first natural frequency depending on the sign of the applied DC voltage. He presented the results of the numerical analysis for a simply supported beam. This problem was more thoroughly discussed in the papers [18-19]. Waisman and Abramovich investigated the simply supported and clamped-free beams with one and two sets of the PZT actuators. They concluded that the stiffening effect generated by the piezoelectric actuators ensures the control of the natural frequency and mode shapes of the tested beams. A similar analysis is presented

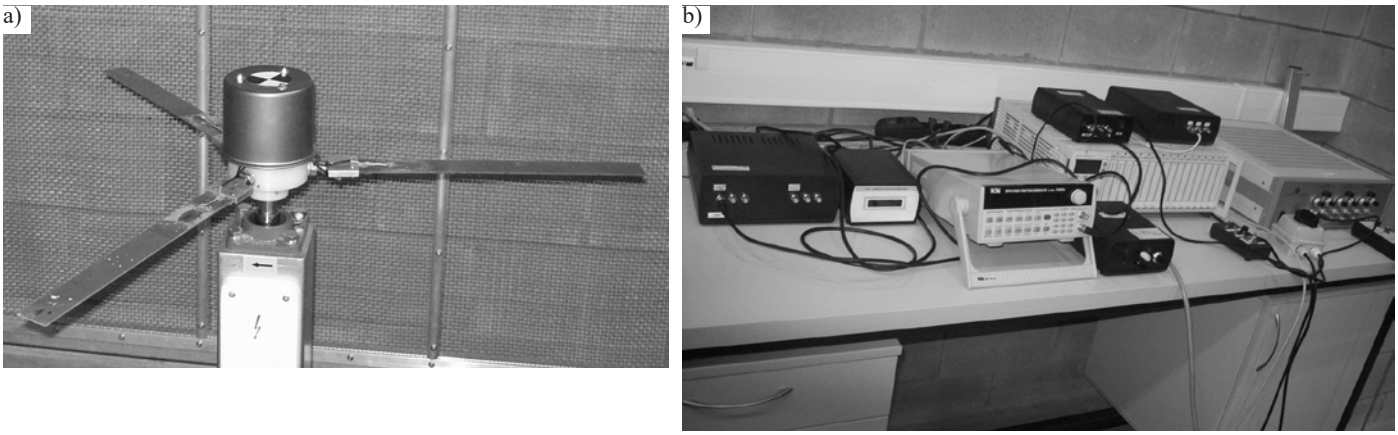

Fig. 1. Views of the tested rotor (a) and electronic equipment(b)

in the paper [8], but the object of the research was a thin plate with PZT actuators.

The aim of this paper is to determine the relation between the dynamics of a rotor blade with MFC elements in relative motion and the rotational movement of the hub. Constant angular velocity can generate undesired changes in the natural frequencies and/or eigenmodes of the active composite blades. The aim of the experimental research was to demonstrate the possibility of using the MFC actuator for reducing these changes.

2. The experimental setup

The experimental studies were performed using a specially designed test stand which is shown in Fig. 1. This stand was built at the Department of Applied Mechanics at the Lublin University of Technology. The rotor (Fig. 1) consisted of a hub with three composite blades which were located 120 degrees relative to each other. The rotor blades were beams with a rectangular cross-section made of glass-epoxy laminate.

The mechanical properties of the glass-epoxy laminate were as follows:

- Young's modulus in fibre direction (i.e., direction 1): 46.43 GPa and in transverse direction of the fibers (i.e., direction 2): 14.926 GPa, respectively,
- Poisson's ratio in plane 1-2: 0.27,
- shear modulus in plane 1-2: 5.233 GPa,
- density: 2032 kg/m^3.

Each blade was composed of six layers. The lay-up configuration of the laminate was: $[\pm 45/90]_S$. The geometry of the rotor blades is given in Table 1.

Table 1. Geometrical dimensions of rotor blades in mm

Length	Width	Thickness
350	34	1.80

The rotor hub was driven by a DC motor. In addition, the sensors and actuators were fixed on the opposite surfaces of the beams. The strain-gauges and piezoelectric actuators were used to measure and control the dynamics of the rotor blades in their relative motion. In our case, the Macro Fiber Composite active elements were used as actuators. They were MFC elements type M-8528-P1. In this case, the piezoelectric d_{33} effect occurs [15]. Each element can be powered by electric current in the range of -500 to 1500 volts.

The piezoelectric properties of the MFC element depend on its dimensions. According to the literature [16], the optimal value of the d_{33} parameter for MFC M-8528-P1 elements is $1.01*10^{-7}$ m/V. The coefficient of permittivity is $8*10^{-9}$ F/m. The mechanical properties of the MFC element were:

- Young's modulus in fibre direction (i.e., direction 1): 15.857 GPa and in transverse direction of the fibers (i.e., direction 2): 30.336 GPa, respectively,
- Poisson's ratio in plane 1-2: 0.31,
- shear modulus in plane 1-2: 5.515 GPa,
- density: 5440 kg/m^3.

Fig. 1(b) shows the electronic equipment which was used to control the power of the electrical motor and piezoelectric transducers. Additionally, the DSP subsystem was used.

3. The numerical model of the rotor

The numerical model of the rotor was designed by the finite elements method using the commercial system Abaqus [1]. The FE model of the rotor is shown in Fig. 2.

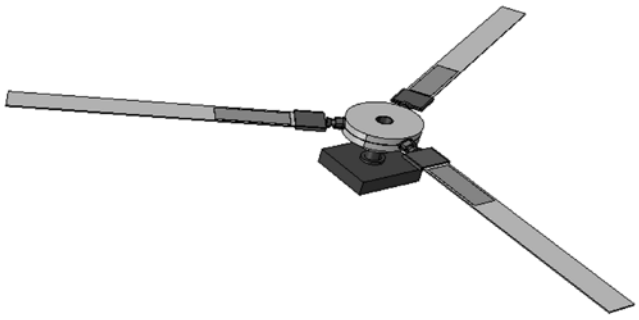

Fig. 2. Numerical model of the active rotor

The model consists of a base with electric drive, the hub with a drive shaft, a blade handle, three composite blades and MFC active elements [16]. The hub and the base of the rotor were built of 10-node tetrahedral, solid elements having three translational degrees of freedom at each node (i.e., C3D10 elements in the Abaqus system). The FE model of the blade handle was built using 20-node (2nd order) solid elements having three translational degrees of freedom at each node (i.e., C3D20R elements). The numerical model of the composite blade was made using 8-node (2nd order) continuum shell elements having three translational degrees of freedom at each node with reduced integration (i.e., SC8R elements). The layup-ply technique was used to made individual layers of the blades. The FE model of the MFC element was constructed using 20-node (2nd order) solid elements, having three translational degrees of freedom at each node and one extra degree of freedom associated with the piezoelectric properties (i.e., C3D20E elements). The combination of all parts of the model was

realized by defining interactions as "TIE" [1]. Mechanical boundary conditions of the model were realized by restraining the nodes located at base translational degrees of freedom. The rotation of the shaft were possible but the base of the rotor was fixed.

4. Influence of the hub rotary velocity on the blade dynamics

The influence of the centrifugal force on the blade dynamics was tested in relative motion. In the experimental studies, the rotating system had a constant rotational velocity denoted as n. The piezoelectric actuator was used to excite the system. The Single Input Single Output procedure was applied, which means that only one blade was excited and its response was measured at one point. In this paper, the experimental results for one blade are reported. The blade was excited using an MFC element powered by a sine sweep signal. Generally, supply voltage can be written as a function:

$$U_A(t) = A\sin\left(\omega_0 t + \frac{1}{2}\varepsilon_A t^2\right) \tag{1}$$

where: A is the amplitude of a sine signal, t is time, ω_0 and ε_A are the initial frequency and angular acceleration, respectively. Both parameters describe the change in the frequency of the signal realized by the MFC actuator. The frequency ω_A of the sine function changes linearly, in the following way:

$$\omega_A(t) = \omega_0 + \varepsilon_A t \tag{2}$$

In the experimental studies, the realization of the time sweep sine was defined as: $t \in \langle 0,30 \rangle s$. In this time, the range of frequency was slowly changed from 8 Hz to 15 Hz (i.e., $\omega_0 = 16\pi$ rad/s, $\varepsilon_A = \frac{7\pi}{15}$ rad/s^2 in Eq. (2)). The frequency range of the MFC excitation signal is illustrated in Fig. 3. The amplitude of the voltage supply signal denoted as A in Eq.(1) was 400 V. The obtained final time series of the voltage supply signal is presented in Fig. 4.

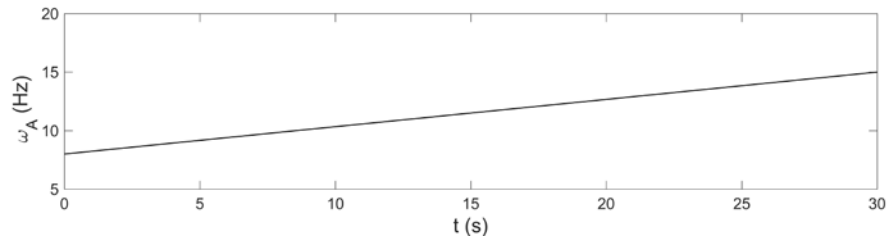

Fig. 3. Frequency change in the MFC excitation signal

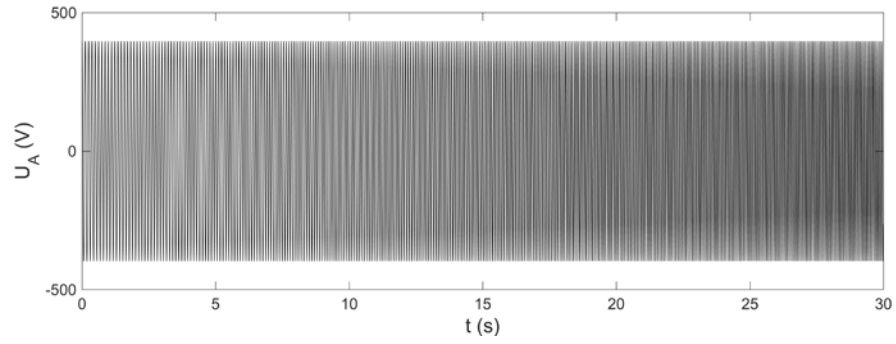

Fig. 4. Time series of the voltage supply of the MFC actuator

The rotation of the blades caused measurement problems. In the first step, the fast speed cameras were used as a non-contact system. However, this test method did not enable taking precise measurements of the rotating blades. In the second step, the strain-gauges were used. The

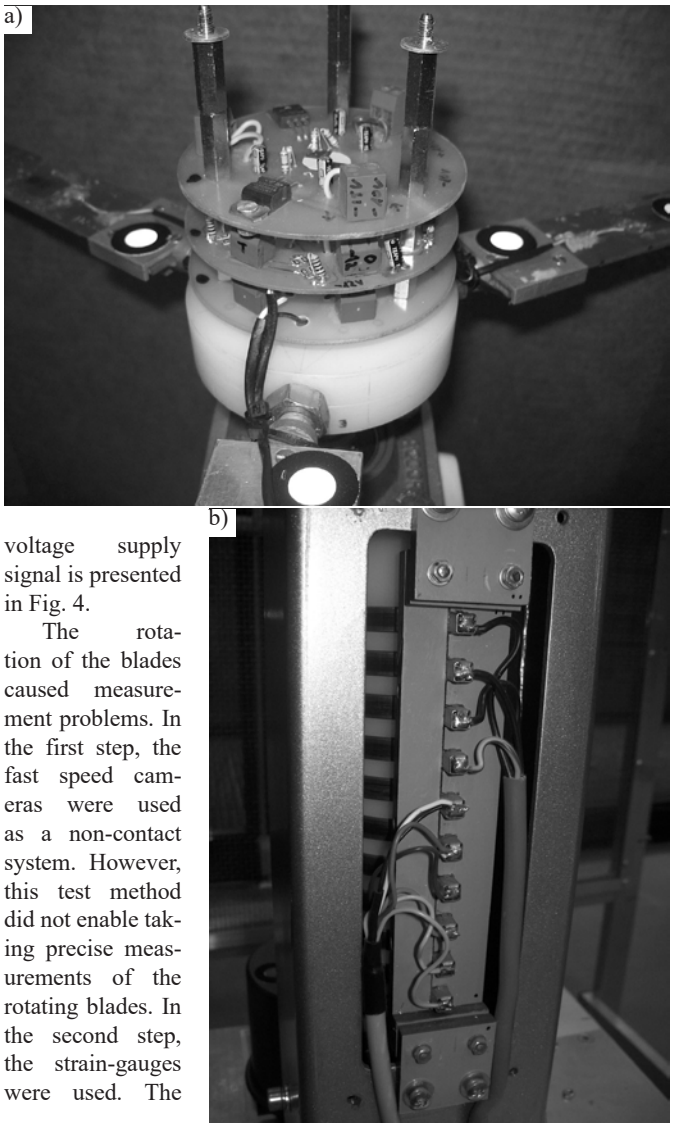

Fig. 5. Views of selected elements of the test stand: (a) electronics system, (b) slip rings

Wheatstone bridge circuit was located on the hub (Fig. 5a). The signals from the rotor were transmitted through the slip rings (Fig. 5b). Therefore, in this paper the strain-gauge signal (denoted as U_S) is given in volts.

The experimental studies were performed with the constant rotational velocity set to 0, 100 rpm, 200 rpm, 300 rpm, 400 rpm, 500 rpm. The response of the blades forced by the MFC element was changing with increasing the rotational velocity (Fig. 6). In the first case, the maximum response of the strain-gauge signal was at 5.49 s (Fig. 6a). In the second case, the maximum response of the strain-gauge signal was at 10.0217 s (Fig. 6b). The natural frequency of the first bending mode (denoted as ω_1) was determined as follows:

$$\omega_1 = \omega_0 + \varepsilon_A t_m \tag{3}$$

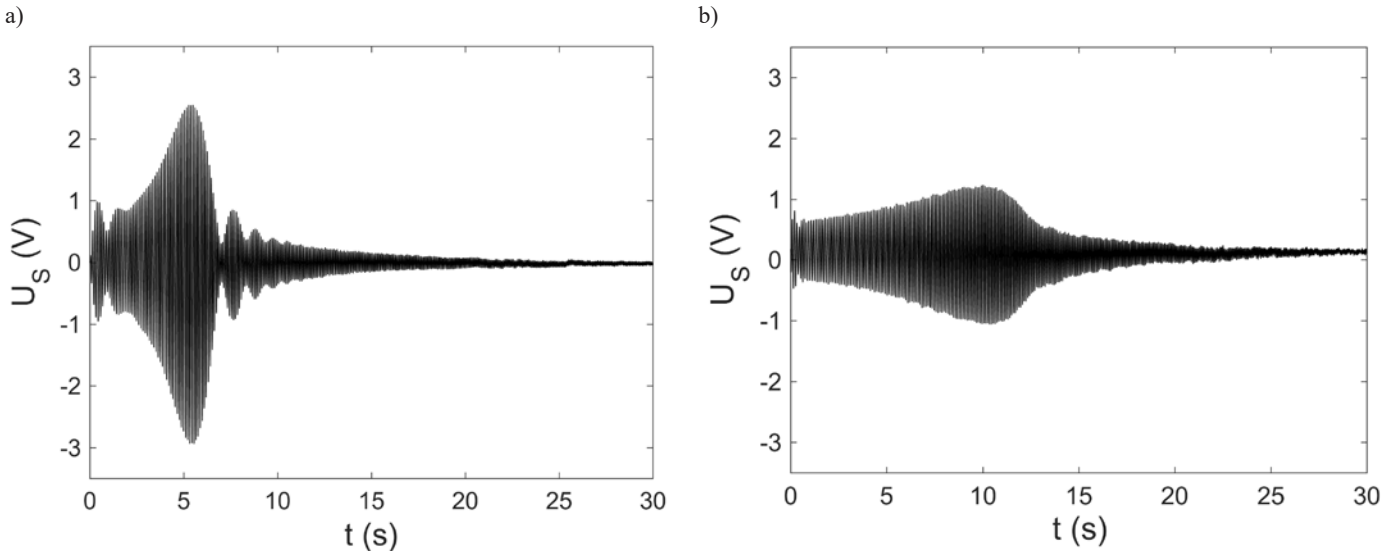

Fig. 6. Strain-gauge signal vs. time, when the rotational velocity was: (a) 0 (b) 200 rpm

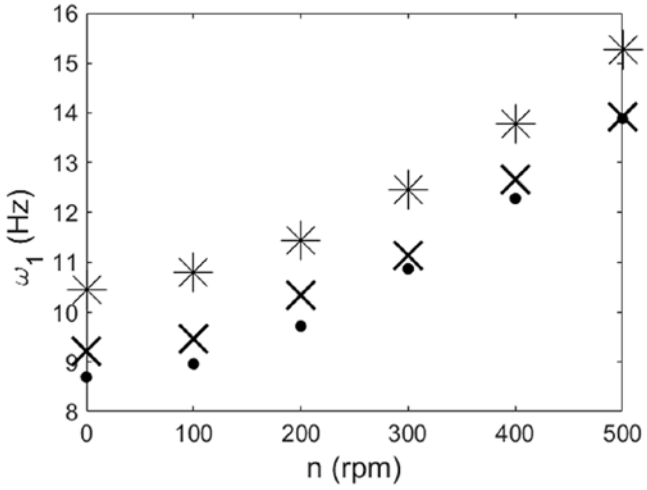

Fig. 7. First bending natural frequency vs. rotational velocity. The numerical solutions are marked by stars (FE-model with MFC elements) and dots (FE-model without MFC elements), respectively. The experimental results are marked by crosses

where: t_m is a time when the amplitude of blade vibration is the maximum.

The obtained experimental values of the first bending natural frequency are shown in Fig. 7. Next, a comparison of the experimental results and the numerical solutions for the lowest bending mode of free vibration was made (Fig. 8). In the FE analysis, the eigen-frequencies and the corresponding modes of free vibration were determined using the Lanczos method [1]. Rotation with a constant angular velocity generates a constant centrifugal force. This effect was taken into account in the FE model by introducing mechanical load. The simulations were made for a selected angular velocity. The FE results for the first five vibration modes, when the angular velocity was 500 rpm, are illustrated in Fig. 8.

The FE results are given in Table 2. These results reveal the impact of the centrifugal force on the resonance area shift. An increase in the natural frequencies was calculated when the angular velocity was 500 rpm (denoted as $\omega_{\max}^{FEM}$) or 0 (denoted as $\omega_{\min}^{FEM}$). The percentage increase in the frequencies was defined as:

$$\delta\omega^{FEM} = \frac{\omega_{\max}^{FEM} - \omega_{\min}^{FEM}}{\omega_{\min}^{FEM}} \quad 100\% \tag{4}$$

In this case, the percentage increase in the frequencies was: 46 %, 9 %, 4 % for the first, second and third vibration modes (Figs. 8a, b, c and Table 2) and 0 % for other modes (Figs. 8 d, e and Table 2), respectively.

The experimental findings are closer to the numerical results when the piezoelectric elements are not included in the FE model. A very good agreement for all methods was achieved. The details are given in Fig. 7. The obtained characteristic demonstrates that the natural frequency of the first bending mode increases with increasing

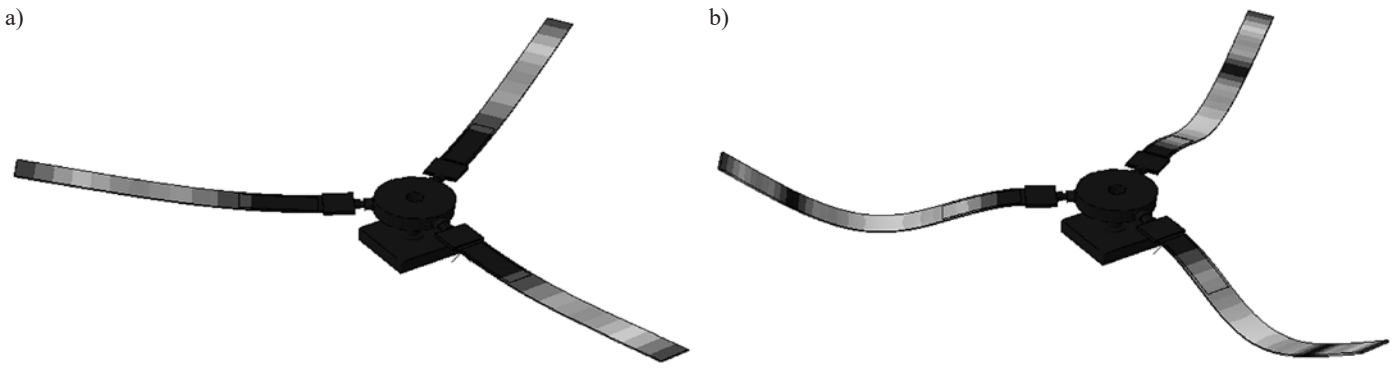

Fig. 8. Free vibration modes when the angular velocity is 500 rpm (a) (b) - first, second in plane bending modes

c)

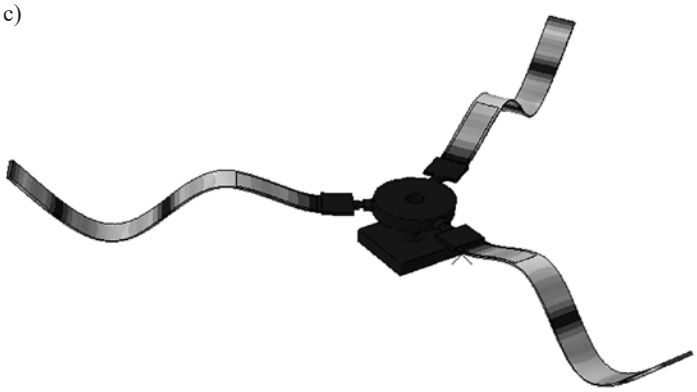

d)

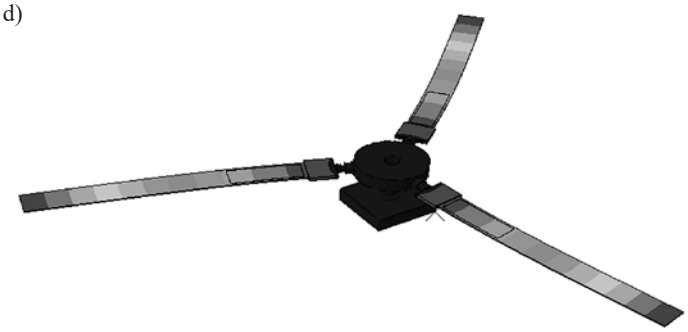

e)

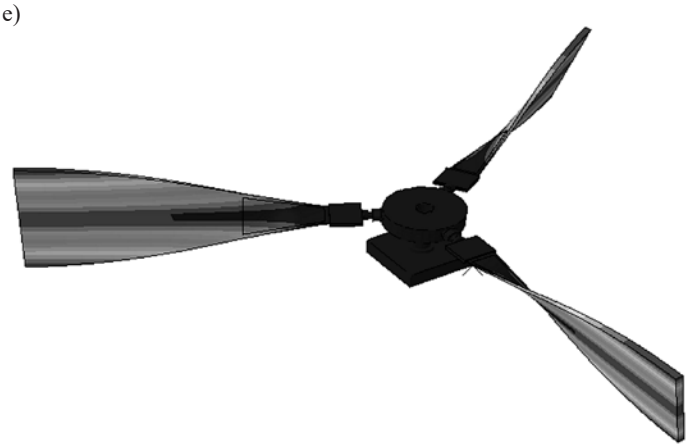

Fig. 8. Free vibration modes when the angular velocity is 500 rpm (c) - third in plane bending modes, (d) - first out of plane bending mode and (e)- first torsion mode

the rotational velocity. This is the centrifugal stiffening effect. Unfortunately, the strain-gauge can only verify the first mode vibrations. For higher natural frequencies, the signal from the strain-gauge is close to the level of noise. In the case of the experimental studies, the increase in the value of the first natural frequency versus the rotational velocity [7] can be described by:

$$\omega_1(n) = \sqrt{\omega_{\min}^2 + \left(\frac{n}{n_{\max}}\right)^2 \left(\omega_{\max}^2 - \omega_{\min}^2\right)} \qquad (5)$$

where: n is the analyzed rotational velocity, ω_{min} is the experimental value of the natural frequency when the rotor is fixed, ω_{max} is the experimental value of the natural frequency when the tested angular velocity is maximum n_{max}= 500 rpm.

Both values can be read from Fig. 7. The final form of Eq. (5) can be written as:

$$\omega_1(n) = \sqrt{a + bn^2} \qquad (6)$$

where: a and b are new constants.

Table 3 lists the values of the parameters a and b calculated by Eq. (5). These parameters were called strict values in Table 2. They were calculated based on two experimental points when the angular velocity was 0 or 500 rpm (Fig. 7). Further, these parameters were estimated using the nonlinear least squares solver in the Matlab software (lsqcurvefit function) [13]. In this case, all experimental points were taken into account. Both methods can be applied because the parameters a and b are almost the same. Eq. (5) helped describe the centrifugal stiffening effect very well.

Table 3. Comparison of the parameters a and b

Parameter	Strict values $a = \omega_{\min}^2$, $b = \frac{\omega_{\max}^2 - \omega_{\min}^2}{n_{\max}^2}$	Values estimated by Matlab	Error in %
FE model with MFC actuator			
a	109.1816	110.7562	1.4
b	0.0004953	0.000491	0.9
FE model without MFC actuator			
a	75.6117	75.7407	0.17
b	0.0004686	0.0004687	0.03
Experimental results			
a	84.9715	86.4554	1.7
b	0.0004351	0.00043799	0.7

Table 2. Natural frequencies vs. rotational velocity in FE analysis

Rotational velocity in rpm	Natural frequency ω^{FEM} in Hz				
	First in plane bending mode	Second in plane bending mode	Third in plane bending mode	First out of plane bending mode	First torsion mode
0	10.5	58.6	157.6	94.6	209.1
100	10.8	58.8	158.9	94.6	209.1
200	11.5	59.5	159.5	94.6	209.1
300	12.5	60.5	160.5	94.6	209.2
400	13.8	61.9	161.8	94.6	209.4
500	15.3	63.7	163.6	94.6	209.5

5. Influence of the MFC actuator on the blades dynamics

A change in the dynamic properties of the blades during rotation may be undesired. So, the initial stress and deflection of the blades can be induced using MFC elements. In this case, the piezoelectric actuator was powered by constant voltage. When placed asymmetrically (only on one side of the beam), the actuator produces a bending effect. It may have an impact on the beam dynamics. Therefore, successive tests were performed when one MFC actuator was powered by the following signal:

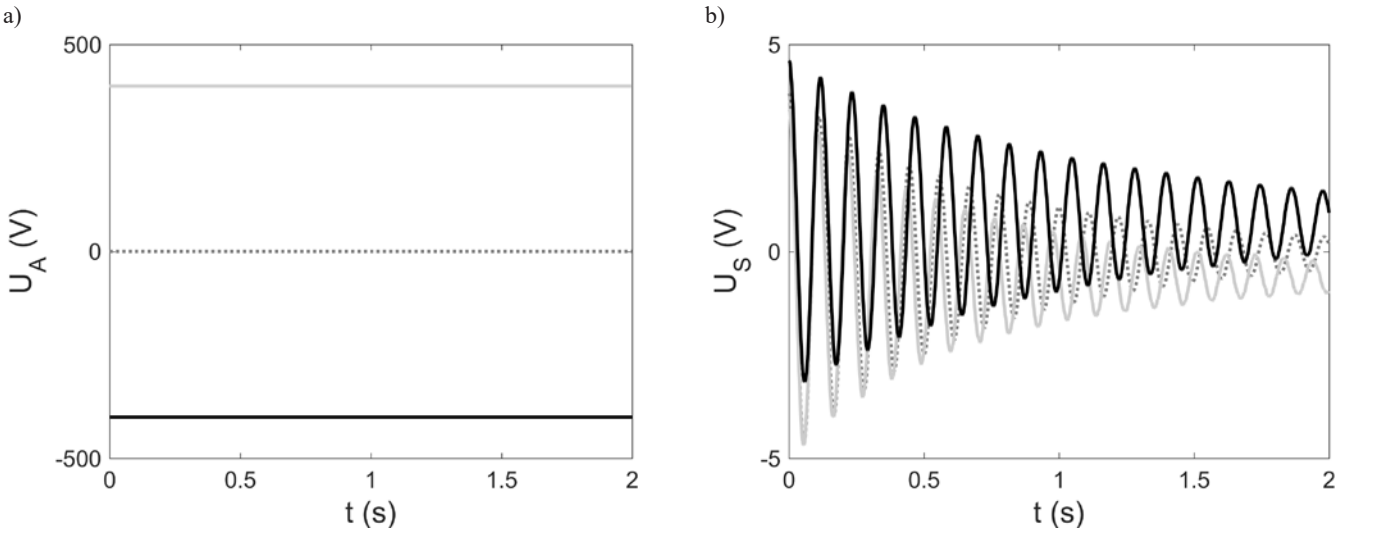

Fig. 9. Power supply voltage of the MFC element (a) and beam responses during the impact test (b) where: gray line - A_0= 400 V, dot line - A_0= 0 and black line - A_0= −400 V

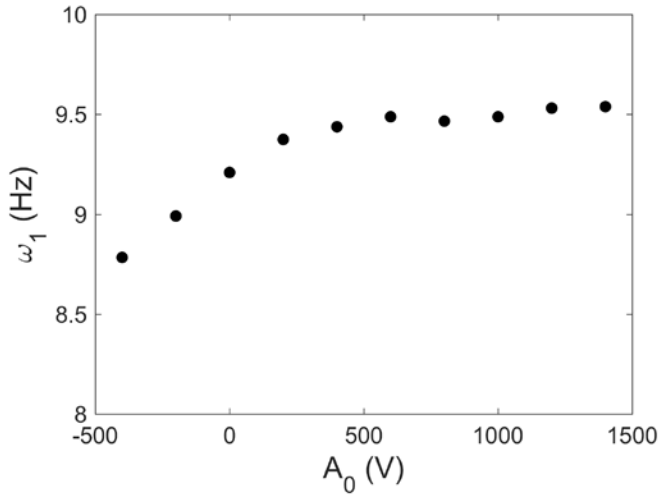

Fig. 10. First natural frequency of the blade vs. voltage parameter A_0 in the impact test

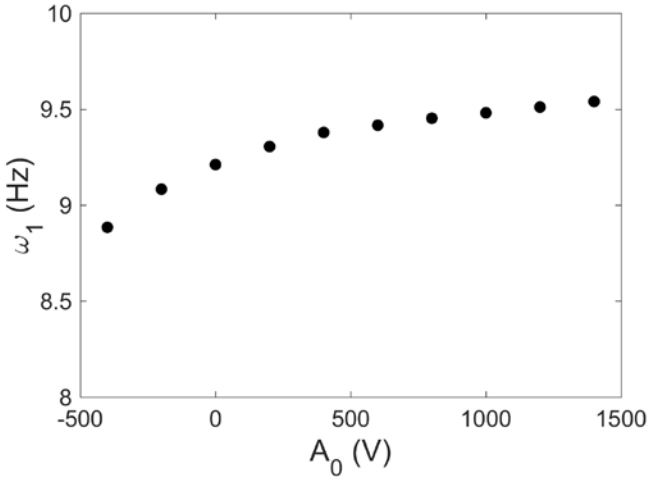

Fig.11. First natural frequency vs. voltage parameter A_0 in the sine sweep test

$$U_A(t) = A_0 \tag{7}$$

where: A_0 is a constant term, offset of the voltage.

The effect of the constant voltage parameter A_0 (Eq.(7)) on the first natural frequency was determined using the impact test. This test was performed when the constant value A_0 was changed from −400 V to +1400 V at 200 V. During the tests, the rotor was fixed. The actuator was supplied with constant voltage (Fig. 9a). The blade was excited using a modal hammer. A short fragment of the recorded signals from the selected impact tests is shown in Fig. 9b. Different voltage levels cause a change in the vibration period. A negative voltage led to an increase in the period of oscillation, in contrast to the case when the voltage parameter A_0 is 0. This can be called a softening effect (Fig. 9b). On the other hand, a positive voltage made this period decrease. This is a stiffening effect (Fig. 9b). All results are shown in Fig. 10. In the considered object, the use of the MFC actuator led to changing the frequency of free vibration by about ±0.5 Hz.

Next, the MFC actuator was used simultaneously for the control of the natural frequency (Eq.(7)) and vibration excitation (Eq.(1)). It is a sine sweep test. The supply voltage can be written as a function:

$$U_A(t) = A_0 + A\sin\left(\omega_0 t + \frac{1}{2}\varepsilon_A t^2\right) \tag{8}$$

The following parameters were applied: A_0 was changed from −400 V to 1400 V at 200 V, A was 100 V, $\omega_0 = 16\pi$ rad/s, $\varepsilon_A = \frac{7}{15}\pi$ rad/s^2. A selection of the applied signals U_A is given in Fig. 12a, whereas the blade responses are shown in Fig. 12b. Natural frequencies were determined using a time series. The results are shown in Fig. 11. The rotor was fixed.

Both methods led to obtaining a similar relation between the first natural frequency and the voltage parameter A_0 (see Figs. 10 and 11).

The possibility of control of the first bending natural frequency by the application the MFC actuator should ensure a partial reduction of the centrifugal stiffening effect. Therefore, the final stage of testing was to analyze the experimental case taking into consideration the above two. Thus, the rotor had a constant angular velocity and the MFC actuator was used for vibration excitation and the control of resonant frequency. The applied voltage signals U_A are shown in Fig. 12a. The following parameters were applied: A_0, was -400 V, 0 or

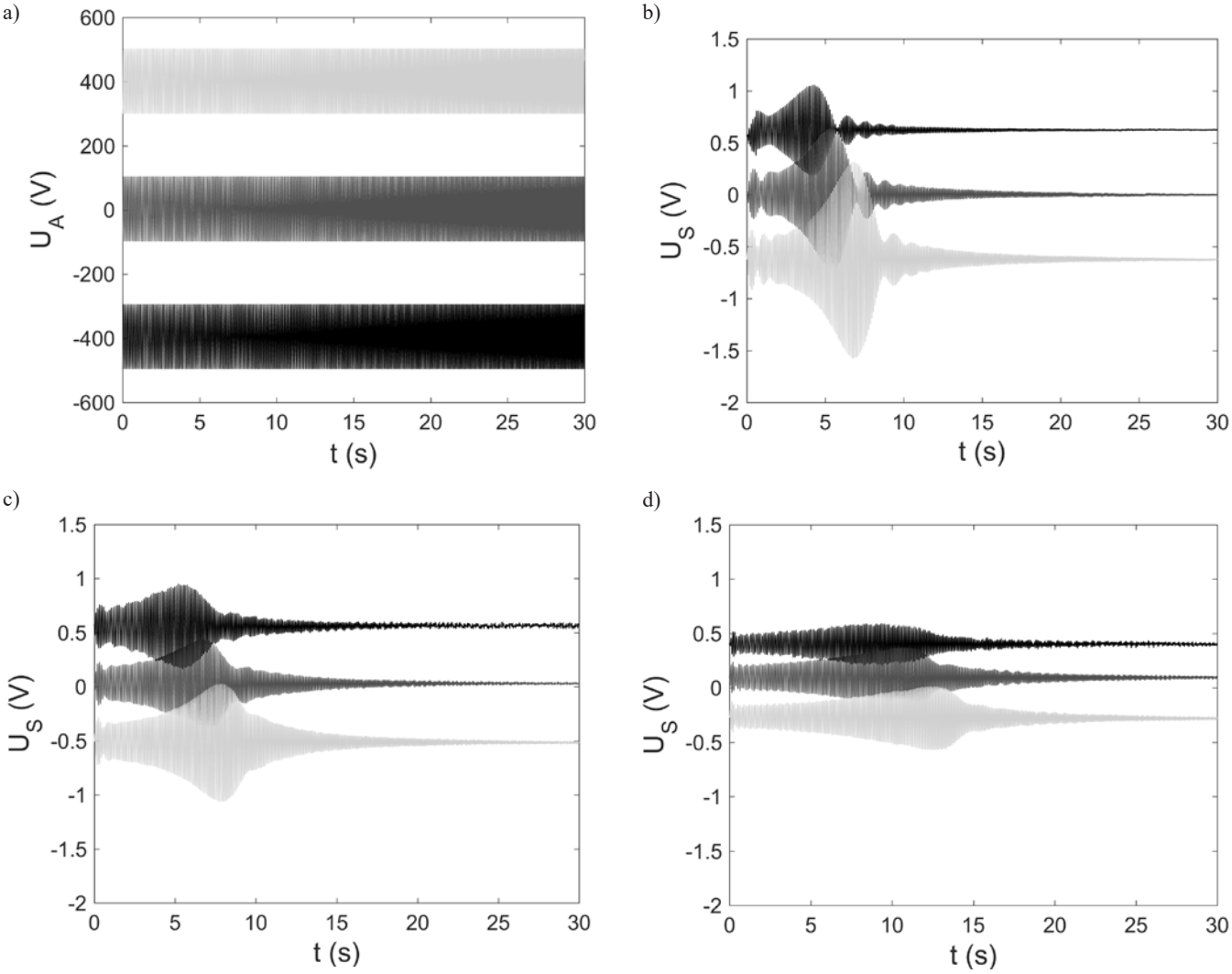

Fig. 12. Experimental results: supply of the MFC actuator (a) and blade response when the angular velocity was: 0 (b), 100 rpm (c) and 200 rpm (d)

+400 V, A was 100 V, $\omega_0 = 16\pi$ rad/s, $\varepsilon_A = \frac{7}{15}\pi$ rad/s^2 and the time window: $t \in \langle 0,30 \rangle s$. The signals from the strain-gauge at different angular velocities are given in Figs. 12b, c, d.

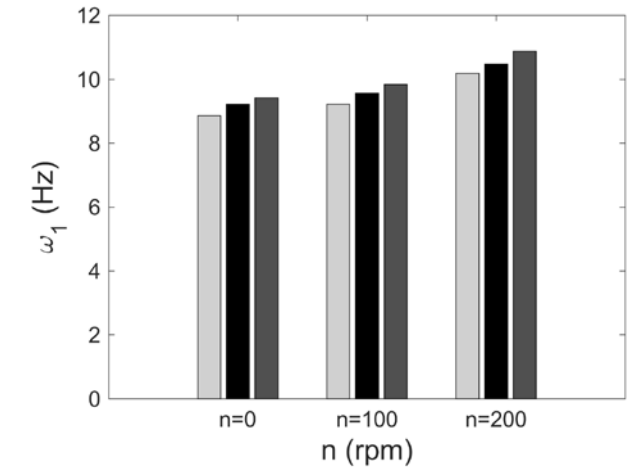

Fig.13. First natural frequency vs. rotational velocity n and control voltage parameter A_0 black color - A_0= 0, brown color - A_0= 400 V, gray color - A_0= -400 V

Using the previously described procedure (Eq. (3)), the natural frequencies were determined for a selected voltage parameter A_0 and rotating velocity. The results are shown in Fig. 13. The value of the voltage parameter A_0 was important and shifted the resonance area. The initial stresses and displacements contributed to a small change in the value of the first bending natural frequency [8, 9, 18, 19]. The active stiffening/softening effect depended on the size and position of the piezoelectric actuator. In our case, the MFC was small and was installed on one side of the blade. This may influence the results given in Fig. 13.

In the numerical study, the MFC actuator was modeled as a deformable body. It was a solid where two opposite walls were electrodes. Piezoelectric material was defined using the standard procedure in the Abaqus software [1]. This approach described the piezoelectric element in a macro scale, but the MFC actuator was not a monolithic crystal. In fact, it was a very complex structure where the PZT fibers as electrodes produce many cells. For example, the active element M-8503-P1 consists of 170 sections distant by 0.5 mm from each other [11]. The equivalent model based on the linear constitutive equation [6, 10]:

$$\begin{aligned} \varepsilon &= S\sigma + dE \\ D &= d\sigma + \xi E \end{aligned} \tag{9}$$

The mechanical phenomenon is described by: strain – ε, stress – σ and compliance – S. In the electrical domain, the following physical

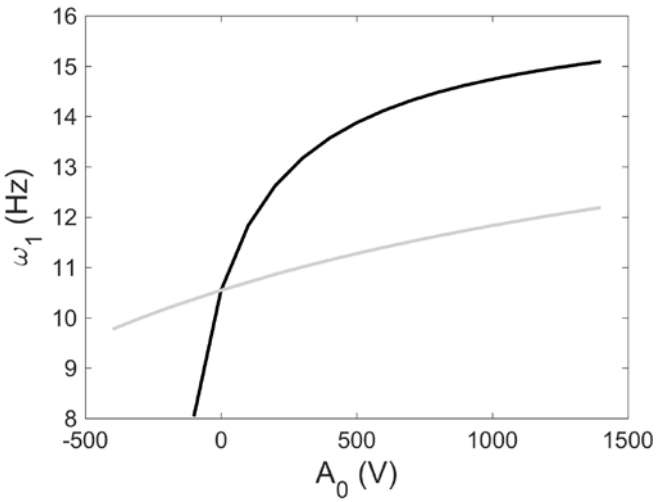

*Fig. 14. First natural frequency vs. parameter d_{33}. Black color – d_{33}= 1.01*10^{-7} m/V, gray color – d_{33}= 1.01*10^{-8} m/V*

parameters are applied: electrical field – E, electric charge – D and permittivity – ξ.

Both equations are coupled by an electromechanical coupling coefficient. The numerical modal analysis was performed, where one MFC actuator was powered by constant voltage. In the numerical model, the voltage-powered MFC element was defined by electrical boundary conditions. Fig. 14 shows the natural frequency of the first mode from the numerical analysis for different values of the coupling coefficient d_{33}. These curves reveal that the active stiffening effect depends on the value of the parameter d_{33}. In the literature [16], this parameter for MFC-8528-P1 was 1.01*10^{-7} m/V. Its value was estimated using the free strain test and the blocking force test. Finally, in the paper [11] this parameter was validated by a comparison of the maximum static deflection using numerical and experimental studies. However, the experimental results (Figs. 10 and 11) are closer to the numerical solution, when the parameter d_{33} was 1.01*10^{-8} m/V. This may be due to the fact that the applied model does not consider phenomena in a micro-scale. Additionally, this parameter cannot be maintained constant in the static and dynamical studies.

6. Conclusions

In the paper, the model of three blade rotor was presented. The experimental and numerical studies were conducted. The analysis investigated the phenomena of the centrifugal stiffening effect and piezoelectric stiffening/softening effects. The following conclusions were formulated:

a) When the rotational velocity was increased, the value of the first bending natural frequency of the blades increased too. The maximum change induced by the centrifugal stiffening effect was 4.7 Hz (Fig. 7, experimental data), when the angular velocity was changed from 0 to 500 rpm.
b) A constant voltage supply to the MFC actuator caused initial stresses/deflections, their value depending on the parameter A_0. This piezoelectric effect can generate a change in the value of natural frequency. The observed change in the first bending mode of the blade was about ±0.5 Hz. The nature of the changes (i.e., increase or decrease) depends on the voltage sign (Figs. 10 and 11).
c) The rotational velocity and the control voltage parameter A_0 are vital . Both parameters can interact with each another and can change the frequency of the first vibration mode. This effect was demonstrated in Fig. 13. However, the applied control voltage parameter A_0 is hardly effective.

The experimental findings were compared and confirmed by the results of the numerical anaZlysis by the finite elements method. The simulations were performed by the Abaqus software package. The studies on the active rotor will be continued in the future.

Acknowledgment

This research is financially supported by the Polish National Science Center under the research grant no. DEC2012/07/B/ST8/03931.

References

1. Abaqus 6.14 documentation.
2. Bilgen O, Wang Y, Inman D J. Electromechanical comparison of cantilevered beams with multifunctional piezoceramic devices. Mechanical Systems and Signal Processing 2012; 27: 763-777, https://doi.org/10.1016/j.ymssp.2011.09.002.
3. Brockmann T H. Theory of Adaptive Fiber Composites >From Piezoelectric Material Behavior to Dynamics of Rotating Structures. Springer Dordrecht Heidelberg London New York, 2009.
4. Brown G V, Kielb R E, Meyn E H, Morris R E, Posta S J. Lewis research center spin rig and its use in vibration analysis of rotating systems. NASA technical paper 2304, 1984.
5. Chaudhari N.B. Dynamics characteristics of wind turbine blade. International Journal of Engineering Research & Technology 2014; 3: 168-173.
6. Chopra I, Sirohi J. Smart structures theory. First edition. New York: Cambridge University Press, 2013. https://doi.org/10.1017/CBO9781139025164.
7. Chromek L. Design of the blisk of an aircraft turbojet engine and verification of its resonance free operation. Applied and Computational Mechanics 2016; 10: 17-26.
8. Hernandes J A, Almeida S F M, Nabarrete A. Stiffening effects on the free vibration behavior of composite plates with PZT actuators. Composite Structures 2000; 49: 55-63, https://doi.org/10.1016/S0263-8223(99)00125-7.
9. Kuo S Y. Stiffening effects on the natural frequencies of laminated beams with piezoelectric actuators. Journal of Aeronautics, Astronautics and Aviation 2010; 42: 67-72.
10. Latalski J. Modelling of a rotating active thin-walled composite beam system subjected to high electric fields. W: Advanced Methods of Continuum Mechanics for Materials and Structures, K. Naumenko, M. Assmus (eds.), Springer, Singapore 2016; 435-455, (ISBN 978-981-10-0958-7), https://doi.org/10.1007/978-981-10-0959-4_24.
11. Latalski J. Modelling of macro fiber composite piezoelectric active elements in Abaqus system. Eksploatacja i Niezawodnosc - Maintenance and Reliability 2011; 52(4): 72-78.
12. Latalski J, Bocheński M, Warmiński J, Jarzyna W, Augustyniak M. Modelling and simulation of 3 blade helicopter's rotor model. Acta Physica Polonica A 2014; 125(6): 1380-1383, https://doi.org/10.12693/APhysPolA.125.1380.
13. MathWorks documentation. <http://www.mathworks.com/help.html> (28.12.2016).

14. Sodano H A, Park G, Inman D J. An investigation into the performance of macro fiber composites for sensing and structural vibration applications. Mechanical Systems and Signal Processing 2004; 18: 683-697, https://doi.org/10.1016/S0888-3270(03)00081-5.
15. Smart Material. <http://www.smart-material.com/MFC-product-main.html> (28.12.2016).
16. Teter A, Gawryluk J. Experimental modal analysis of a rotor with active composite blades. Composite Structures 2016; 153: 451-467, https://doi.org/10.1016/j.compstruct.2016.06.013.
17. Truong K V, Yeo H, Ormiston R A. Structural dynamics modeling of rectangular rotor blades. Aerospace Science and Technology 2013; 30: 293-305, https://doi.org/10.1016/j.ast.2013.08.014.
18. Waisman H, Abramovich H. Active stiffening of laminated composite beams using piezoelectric actuators. Composite Structures 2002; 58: 109-120, https://doi.org/10.1016/S0263-8223(02)00035-1.
19. Waisman H, Abramovich H. Variation of natural frequencies of beams using the active stiffening effect. Composites Part B: Engineering 2002; 33: 415-424, https://doi.org/10.1016/S1359-8368(02)00031-8.

Andrzej MITURA
Jarosław GAWRYLUK
Andrzej TETER
Department of Applied Mechanics
Faculty of Mechanical Engineering
Lublin University of Technology
ul. Nadbystrzycka 36, PL-20-618 Lublin, Poland

E-mails: a.mitura@pollub.pl, j.gawryluk@pollub.pl, a.teter@pollub.pl